CONFERENCE PREPRINT

LOW-THRESHOLD ABSOLUTE PARAMETRIC DECAY INSTABILITY IN X2-MODE ECRH EXPERIMENTS AND THE MISSING POWER EFFECT

E.Z. GUSAKOV
Ioffe Institute
Saint-Petersburg, Russian Federation
email: evgeniy.gusakov@mail.ioffe.ru

A.Yu. POPOV
Ioffe Institute
Saint-Petersburg, Russian Federation

Abstract

A possibility of low-threshold absolute PDI excitation in cases when localization or trapping of daughter waves is not possible in X2 ECRH experiments is considered. The PDIs driven by the pump beam of extraordinary microwaves propagating along a monotonous density profile and leading to the excitation of a couple of electron Bernstein (EB) daughter waves is studied. The decay conditions for such a two-plasmon decays in many toroidal devices could be satisfied in a couple of spatial points thus making possible the daughter wave energy circulation between them and, as a consequence, the onset of the absolute PDI. In the present paper this scenario of absolute PDI is analyzed numerically accounting for the finite width of the pump wave beam. The approximate expression for the absolute PDI threshold dependence on the daughter waves convective losses along the plasma inhomogeneity direction and diffractive losses across the pump beam is obtained. It is shown that the instability power threshold was exceeded under conditions of on-axis X2-mode ECRH experiments at T-10 and TEXTOR, in which the missing power effect was observed.

INTRODUCTION

Electron cyclotron resonance heating (ECRH) and current drive are widely used in toroidal plasmas and considered for neoclassical tearing mode control in ITER. In accordance with the theoretical estimates based on the one-dimensional model [1,2] and obtained in the late 1980s and early 1990s [3,4], the nonlinear effects, first of all parametric decay instabilities (PDIs) that can accompany microwave propagation, were believed to be deeply suppressed due to the fast convective energy losses of daughter waves from the decay region, which has a finite width in inhomogeneous plasmas. However, over the last decade and a half, various anomalous nonlinear phenomena have been found during microwave passage through the plasma volume at levels of auxiliary ECRH heating less than 1 MW in a microwave beam. The most striking evidence of the onset of nonlinear effects was obtained first at TEXTOR [5,6] and then at ASDEX-Upgrade [7,8] and Wendelstein 7-X [9,10], where strong microwave emission shifted down and up in frequency with respect to the gyrotron frequency was observed in a course of X2-mode ECRH experiments. More recently, plasma emission at a frequency about half the pump wave frequency has been detected in X2-mode ECRH experiments at ASDEX-Upgrade [7] and TCV [11]. A convincing demonstration of anomalous ion acceleration at X2-mode ECRH under conditions where the energy exchange between the ion and electron components was negligible has been obtained at TCV and TJ-II [12-14]. Moreover, a substantial broadening of the power deposition profile was demonstrated at T-10 [15], DIII-D [16], L-2M [17] and the missing power or absorbed power lack effect was observed at TEXTOR [18], T-10 [19-23] and TJ-II [22]. The majority of these observations were performed as the launched microwave beam passed through a region of plasma characterised by a non-monotonic density profile. Such a profile is a perpetual feature of the plasma column axis, or can be a consequence of a magnetic island, of a density pump-out effect, or of the presence of ELM filaments and blobs. In this case, it seems that all anomalous phenomena can be interpreted as a result of secondary nonlinear events that accompany the primary low-threshold PDI [24], leading to the excitation of daughter waves trapped in the local maximum of a non-monotonic density profile. The growth of the primary PDI is believed to be saturated due to both secondary decays of daughter waves and depletion of the pump wave. The model proposed in [24] demonstrates that the strong plasma emission, i.e., the spurious signal for microwave diagnostics, is a consequence of the coupling of the various daughter waves and the pump wave. This mechanism appears capable of reproducing the fine details of the frequency spectrum and the absolute magnitude of the emitted radiation [25-29]. It also predicts a significant anomalous absorption in the range of 10 – 70 % in the electron channel, which may be responsible for the broadening of the ECRH power deposition profile [15-17]. Besides, the anomalous heating of ions in the presence of microwaves is explained by the generation of ion modes, which directly transfer pump power to the ion component [30]. However, it is worth noting that anomalous effects such as an evident broadening of the power deposition profile [15-17], as well as a discrepancy between the microwave power launched into the plasma and that deposited into the electron component in the EC resonance layer [18-22], was also found when the density profile between the microwave antenna and the ECR was monotonic. As it was previously evidenced in [31], where the one-dimensional model developed in [1,2] was generalized, the absolute PDI of a pump microwave beam can also occur in the presence of a monotonic density

profile. Such a phenomenon occurs if there are two close decay points for the pump wave and a pair of daughter waves propagating in opposite directions.

In this paper it will be demonstrated that the model proposed and developed in [31] has the capability to elucidate the discrepancy between the microwave power launched into the plasma and absorbed in the EC resonance layer (so called missing power effect) that has been indicated in the X2-mode ECRH experiments at T-10 [19-23]. In the course of these heating experiments, performed under conditions of very large ECR layer optical depth, the dependence of the power fraction actually absorbed in the second harmonic EC resonance on the averaged density has been found. The value of density above which the injected microwave power, as predicted by linear theory [32-36], is fully absorbed by electrons in the X2-mode ECR layer was determined. It was concluded that at smaller plasma density values the linear theory of X2-mode ECR absorption is not valid, and an empirical formula for the ECR layer optical depth was proposed. The qualitative explanation of this effect proposed in the talk [23] utilizes a model based on quasi-linear distortions of the electron distribution function under the ECRH. However, this model faces difficulties when interpreting the absence of the missing power effect at O1-mode ECRH of the T-10 plasma, as reported in [19 – 22]. As it is shown in the present paper, the model [31] allows explaining the dependence of the power absorption efficiency on the plasma density and electron temperature by dependence of the PDI threshold on these quantities.

1. THEORETICAL MODEL

Consider a monochromatic Gaussian microwave beam propagating along the inhomogeneity direction, hereafter denoted by the *x*-coordinate, almost perpendicular to the magnetic field aligned with the *z*-coordinate. In a narrow layer where we assume this pump decays, we represent it using the WKB approximation as follows

$$\mathbf{E}=\frac{w^2}{2\pi}\sqrt{\frac{2P_0}{w^2c}}\int_{-\infty}^{\infty}dk_y dk_z \mathbf{e}_0\left(x,k_y,k_z\right)\sqrt{\frac{\omega_0}{ck_x\left(x,k_y,k_z\right)}}\exp\left(-\frac{k_y^2w^2}{2}-\frac{k_z^2w^2}{2}+i\int^x k_x\left(x',k_y,k_z\right)dx'+ik_z z+ik_y y-i\omega_0 t\right)+c.c. \quad (1)$$

The representation (1) describes a microwave beam propagating from the launching antenna inward the plasma with the pump power P_0 and the beam width w. Assuming that the pump beam is wide and its width obeys the inequality $w>>c/\omega_0$, we neglect the diffraction effect in the decay layer in both the y and z directions, *i.e.*, $k_x(x,k_y,k_z)\approx k_x(x,0,0)$. In the case of an extraordinary wave the wavenumber reads $k_x=\omega_0 n_x/c$ where $n_x=\sqrt{\varepsilon-g^2/\varepsilon}$ is the x component of the refractive index, ε, g are the diagonal and off-diagonal perpendicular components of the cold-plasma dielectric tensor. In its turn, the polarization vector reads $\mathbf{e}_0\approx -ig/\varepsilon\cdot\mathbf{e}_x+\mathbf{e}_y$ where $\mathbf{e}_x,\mathbf{e}_y,\mathbf{e}_z$ - unit vectors that determine the Cartesian coordinate system (x,y,z). In the case of an ordinary wave the x - component of the refraction index is represented as $n_x=\sqrt{\eta}$, where η is the diagonal component of the cold-plasma dielectric tensor along the magnetic field. Taking advantage of the inequality $n_z=k_z c/\omega_0<<1$, we represent the components of the polarization vector as follows $\mathbf{e}_0\approx(\sqrt{\eta}\,n_z\mathbf{e}_x, i\sqrt{\eta}\,n_z\omega_0/\omega_{ce}\mathbf{e}_y,\mathbf{e}_z)$ where ω_{ce} is the electron cyclotron frequency. Here the polarization vector components perpendicular to the magnetic field are small, however, important for providing of the nonlinear coupling for the decay waves.

The decay of the extraordinary wave (1) leads to the excitation of daughter electron Bernstein (EB) waves [24], whose local dispersion equation has the form

$$D_E=q^2+\chi_e(\omega,q)+\omega^2 g(\omega)^2/c^2=0 \quad (2)$$

In equation (2) the last term is due to the electromagnetic contribution in a vicinity of the upper hybrid (UH) resonance, $q=\sqrt{q_\perp^2+q_z^2}$, $q_\perp=\sqrt{q_x^2+q_y^2}$ and q_z are the wavenumber components perpendicular to and aligned with the magnetic field, accordingly, and

$$\chi_e=\frac{2\omega_{pe}^2}{\upsilon_{te}^2}\sum_{m=-\infty}^{\infty}\exp\left(-\frac{q_\perp^2\upsilon_{te}^2}{2\omega_{ce}^2}\right)I_m\left(\frac{q_\perp^2\upsilon_{te}^2}{2\omega_{ce}^2}\right)\left(1+\frac{\omega}{|q_z|\upsilon_{te}}Z\left(\frac{\omega-m\omega_{ce}}{q_z\upsilon_{te}}\right)\right) \quad (3)$$

is the familiar representation for the linear electron susceptibility. In equation (3) υ_{te} is the electron thermal velocity, ω_{pe} is the electron plasma frequency, I_m is the modified Bessel function of the first kind and $Z(\xi)$ is the plasma dispersion function. The potentials of daughter EB waves are determined by means of the WKB approximation as follows

$$\phi_a(\mathbf{r})=\frac{A(y,z)}{2|U_a(x)|^{1/2}}\exp\left(i\int_0^x q_{ax}(\xi)d\xi-i\omega_a t\right)+c.c.,\ \phi_b(\mathbf{r})=\frac{B(y,z)}{2|U_b(x)|^{1/2}}\exp\left(i\int_0^x q_{bx}(\xi)d\xi+i\omega_b t\right)+c.c. \quad (4)$$

where A, B are the amplitudes, $q_{jx} = q_x(\omega_j), j = a,b$ are solutions to the local dispersion equation (2), $\omega_a = \omega_0 - \omega_b$ and $U_{jx} = \partial D_E / \partial q_{jx} \big/ \partial D_E / \partial \omega_j$ stands for the group velocity component along the direction of the plasma inhomogeneity of the corresponding wave *j=a,b*. In inhomogeneous plasmas the decay of the pump wave (1) into EB waves (4) occurs in the vicinity of the point $x = x_d$ where the decay resonance condition for the wavenumbers of nonlinearly coupled waves is satisfied, i.e.,

$$\Delta(x)\big|_{x=x_d} \equiv (q_{bx} + k_{0x} - q_{ax})\big|_{x=x_d} = 0 \quad (5)$$

The system of equations describing the nonlinear excitation of a pair of electron Bernstein (EB) waves (4) due to the decay of the Gaussian extraordinary wave beam (1) can be represented in the following form

$$\begin{cases} i\dfrac{\partial}{\partial t}a + iU_a\dfrac{\partial}{\partial x}a + \Lambda_{ay}\dfrac{\partial^2}{\partial y^2}a + \Lambda_{az}\dfrac{\partial^2}{\partial z^2}a = \nu_0\sqrt{\dfrac{\omega_a}{\omega_b}}\exp\left(-\dfrac{y^2}{2w^2} - \dfrac{z^2}{2w^2} - i2\Psi(x)\right)b \\ -i\dfrac{\partial}{\partial t}b + iU_b\dfrac{\partial}{\partial x}b + \Lambda_{by}\dfrac{\partial^2}{\partial y^2}b + \Lambda_{bz}\dfrac{\partial^2}{\partial z^2}b = \nu_0\sqrt{\dfrac{\omega_b}{\omega_a}}\exp\left(-\dfrac{y^2}{2w^2} - \dfrac{z^2}{2w^2} + i2\Psi(x)\right)a \end{cases} \quad (6)$$

which takes into account convective daughter wave losses in the inhomogeneity direction and two-dimensional diffractive losses across it. In equation (6) $a = w/\sqrt{16T_e}\sqrt{\omega_a \partial D_E/\partial\omega_a}A$ and $b = w/\sqrt{16T_e}\sqrt{\omega_a \partial D_E/\partial\omega_a}B$ are normalized amplitudes of the daughter waves, ν_0 is the nonlinear coupling coefficient determined in the kinetic approximation with due account of spatial dispersion [33], which is of crucial importance for the description of EB waves, $\Lambda_{jy} = \partial D_E / 2\partial q_{jy}^2 \big/ \partial D_E / \partial\omega_j$, *j=a,b* are the diffraction coefficients along the *y*-coordinate, $\Lambda_{jz} = \partial D_E / 2\partial q_{jz}^2 \big/ \partial D_E / \partial\omega_j$, *j=a,b* are the diffraction coefficients along the *z*-coordinate, $\Psi(x) = \int_{x_d}^{x} \Delta(x')dx'$ is the phase due to the mismatch of the decay resonance condition (5) for the numbers of coupled waves in inhomogeneous plasmas. In the following, we assume that the coefficients of the set of partial differential equations (6) are constant and take them according to the temperature and density profiles measured experimentally.

2. LOW-THRESHOLD-PARAMETRIC DECAY OF THE PUMP MICROWAVE IN THE T-10 TOKAMAK X2-MODE ECRH EXPERIMENTS WITH A MONOTONIC DENSITY PROFILE

The T-10 tokamak was a medium-sized circular machine with major and minor radii of R = 1.5 m and a = 0.3 m, respectively. The maximal toroidal magnetic field was B_T = 2.5 T and the plasma current achieved up to I_p = 350 kA. The T-10 tokamak was supplied with an auxiliary electron cyclotron resonance heating (ECRH) gyrotron system with an output power of up to 2.5 MW. From the late 1980s until the facility shutdown, O1- and X2- mode ECRH experiments were conducted at the T-10 tokamak for almost three decades. A huge database of experimental results was collected. In manuscript [19], this database was used to compare the electron heating efficiency at the first and second harmonics of the electron cyclotron (EC) frequency. The main conclusions of the analysis can be formulated as follows. In the O1-mode ECRH experiments the microwave power deposition was found to be in accordance with theory [32], predicting a substantial pump power absorption at a single pass of the microwave beam. On contrary, in the X2-mode ECRH-experiments the fraction of the pump power deposited in the second harmonic of EC-resonance was much smaller than the total pump power, however increased with increasing plasma density. This experimental result contradicts to the opacity estimates for the second EC resonance harmonic in the linear theory [32], predicting optical depth much larger than unity. In experiment, only above a specific threshold plasma density value did the estimation of the actual deposited power approach the launched microwave power, bringing the absorption efficiency in line with theory [34-36]. It was also shown in [19-23] that the density threshold value, at which the estimation of the deposited microwave power approaches the launched pump power, is inversely proportional to the electron temperature. It should be mentioned that in the experiments under consideration the background density profiles
were monotonic. Figure 1 shows typical monotonic density (bottom and left axes) and temperature (bottom and left axes) profiles that were measured in the T-10 tokamak (see figure 12 in [34] and figure 2 in [20], correspondingly). The dashed dotted and dashed lines are the R- and L -cutoff frequencies for the X-mode and given background profiles (see bottom and right axes).Figure 2 shows the one-dimensional dispersion curves of quasi-electrostatic EB daughter waves whose dispersion relation is defined by equation (2) and frequencies $f_a = 69.585$ GHz and $f_b = 70.415$ GHz are slightly below the local upper hybrid frequency. The dispersion curves of the second wave are shifted upward by the number of the extraordinary pump wave with frequency $f_0 = 140$ GHz. The arrows show the EB and slow extraordinary (SX) modes of both waves. There are two close points where the curves corresponding to the EB modes intersect and the decay resonance condition (5) is satisfied.

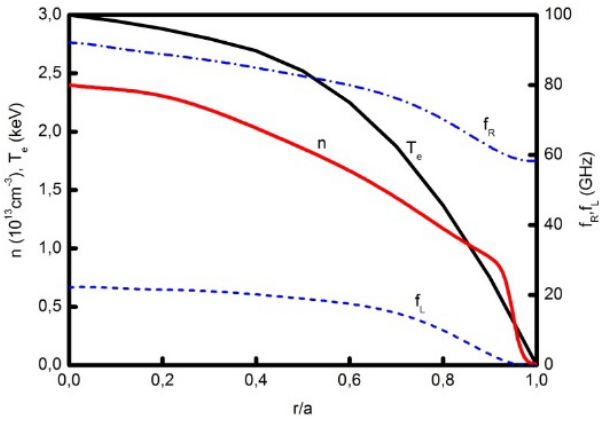

Figure 1. Bottom and left axes: typical monotonic density (figure 12 in [34]) and temperature (figure 2 in [20]) profiles measured in T-10. Bottom and right axes: right (R, dashed dotted line) and left (L, dashed line) cutoff frequencies for the X-mode.

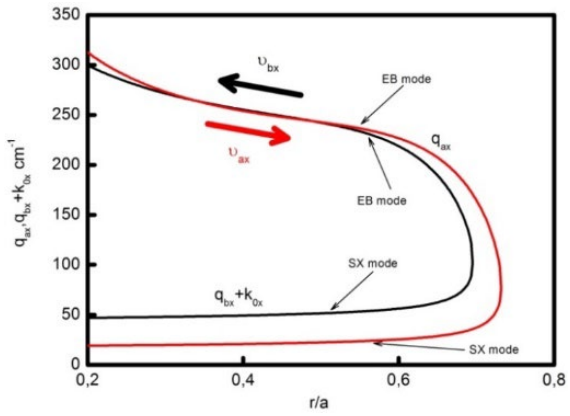

Figure 2. One-dimensional dispersion curves of daughter waves at frequencies f_a=69.585 GHz and f_b=70.415 GHz.

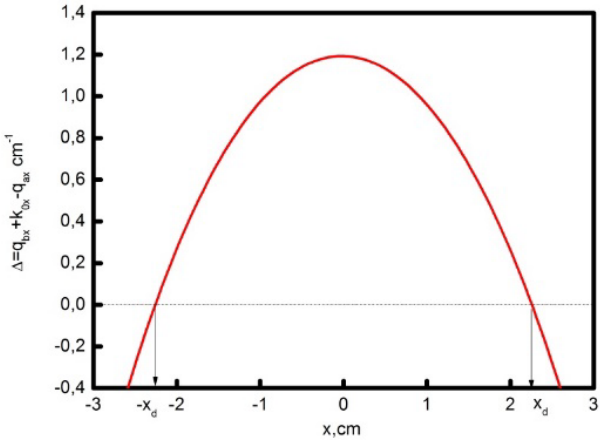

Figure 3. Spatial dependence of the decay resonance condition (6), which is perfectly approximated by a parabola.

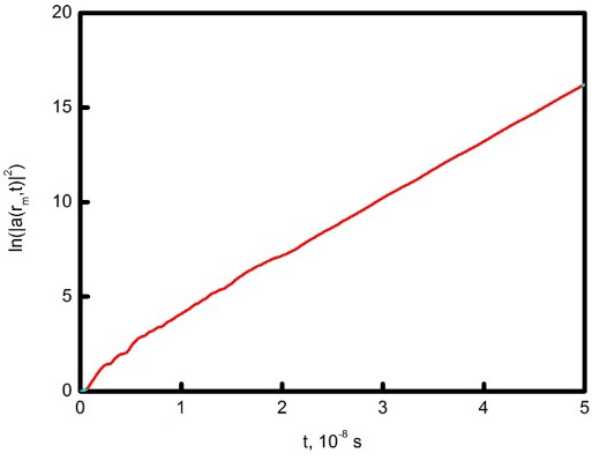

Figure 4. Evolution of the function $\ln|a|^2$ taken at the origin of the coordinate system. The beam width and power are w = 3 cm and P_0 = 0.8 MW, correspondingly.

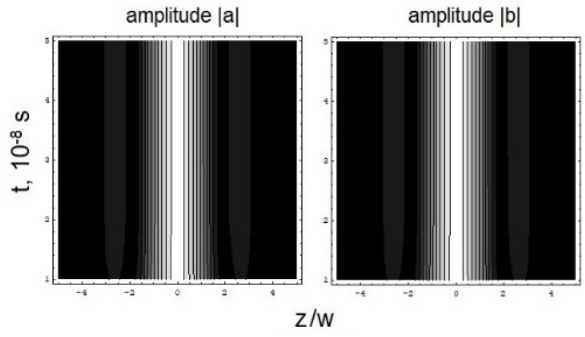

Figure 7. Contour plots illustrating the evolution of normalized amplitudes |a| and |b| of the daughter waves along the z coordinate.

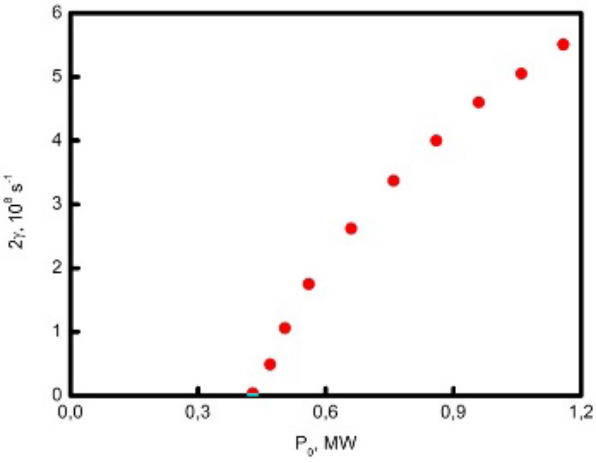

Figure 8. Dependence of the instability growth-rate $2\gamma = d\ln|a|^2/dt$ on the pump power. For the parameters used, the instability threshold is about 0.4 MW.

We further denote these decay points as $\pm x_d$. In this case the decay condition mismatch (5) takes a form $\Delta(x) \approx (x^2 - x_d^2)/l_d^3$, whereas the corresponding phase is given by $\Psi(x) = \int_{x_d}^{x} \Delta(x')dx' = x^3/(3l_d^3) - x_d^2 x/l_d^3$. The group

velocities of the daughter waves are counter-directed, as depicted by the thick arrows. The parameters are taken as shown in figure 1. The off-axis ECR position is assumed. For the pump wave, the second harmonic of the EC resonance is on the high field side at about half the minor radius. Figure 3 shows the spatial dependence of the decay condition mismatch $\Delta(x)$ in a local coordinate system whose origin is at the function Δ extremum and which is used in the set of equations (6). As can be seen, it is perfectly approximated by a parabola. In the case of one-dimensional diffractive losses ($\Lambda_{az} = \Lambda_{bz} = 0$) the system (6) was studied in [31], where it was proved that equations (6) describe daughter EB waves, two-dimensionally localized in the region defined by separation of the decay points and by a finite-width of the pump beam, whose amplitudes grow exponentially in time. This means the excitation of the most dangerous absolute instability of the pump wave (1). Then we assume the beam radius w=3 cm and its power 0.8 MW and solve numerically equations (6) with the coefficients calculated for the profiles shown in figure 1. Figure 4 shows in a semi-logarithmic scale the exponential growth of the energy of the first EB wave $\ln(|a|^2)$. The temporal evolution of the second daughter wave is the same. This temporal growing corresponds to the excitation of absolute PDI. The evolution of spatial structure of the daughter wave amplitudes normalized to their value in the origin is shown in figures 5-7, demonstrating contour plots of the amplitudes $|a|$ and $|b|$ along the x,y,z coordinates, respectively.

The localization of both solutions and the conservation of their distribution in time confirm the excitation of the PDI eigenmodes. The distributions in figures 5-7 have no zeros along all coordinates, which proves that both UH waves correspond to the most dangerous fundamental mode. Varying the beam power, we get the power dependence of the growth rate $2\gamma = d \ln |a|^2 / dt$ shown in figure 8 for the plasma parameters used and the pump beam width w = 3 cm. As it is seen in the figure the instability is very fast whereas the absolute instability threshold in this case is about 0.4 MW, which is substantially smaller than the pump power 800 kW available in one beam at T-10.

By changing the central plasma density and the beam width and solving equations (6), we get the dependencies of the APDI threshold on the mean density shown in figure 9. The grey line indicates the beam power being actually available at T-10 when the tokamak had operated. For it, the PDI density threshold value is about $< n_e^{th} > \simeq 3 \times 10^{13}$ cm^{-3}. With a beam width of 3 cm and density values less than 3×10^{13}cm^{-3}, at which the missing power effect is reported in [19 - 23], the PDI threshold is overcome and the instability develops. It's likely to saturate at a high level. Daughter waves leaving the decay layer and gaining a substantial fraction of the pump power experience the ECR damping far away from the absorption region of the pump wave.As the density increases, the growth rate decreases. Most likely, this leads to a decrease in the saturation level of the instability and in the power fraction acquired by daughter waves. The latter should result in the increase of the pump power absorbed at the second harmonic of the EC resonance. When the averaged density exceeds the value of 3×10^{13}cm^{-3}, the instability is no longer excited. This allows expecting complete absorption of the pump wave in the region prescribed by the linear theory. This value, which will be referred to as the PDI density threshold value, is in agreement with the experimentally discovered 100% power absorption density threshold (see figure 12 in [19], figure 4 in [20]). To explain the decrease in the power threshold with the decrease in the average density, we note that for the range of average densities under consideration, instability occurs in the region where the temperature profile is fairly flat. A decrease in the average density shifts close decay points corresponding to the fundamental PDI eigenmode to the core, toward the fundamental ECR harmonic. This has little effect on the efficiency of nonlinear coupling due to the insignificant change in temperature, but reduces the group velocities of both daughter waves in line with their coordinate dependence $U_j \propto 1 - \omega_{ce}(x_d)/\omega_j$, $j = a,b$ and, as a result, leads to a decrease in the instability threshold.

By setting the beam width and power equal to w = 3 cm and P_0 = 0.8 MW, respectively, and varying the electron temperature, we get the dependence of the PDI density threshold value on the electron temperature shown in figure 10 and matching the experimental dependence of the 100% power absorption density threshold dependence on the electron temperature plotted in figure 3 of [20]. To explain this dependence, we point out that the larger the dimensionless parameter $q_{jx}\upsilon_{te}/\omega_{ce}$, characterizing the role of spatial dispersion of plasma perpendicular to the magnetic field in the description of the EB wave, the lower the nonlinear coupling of the extraordinary wave with two EB waves (see figure 2 in [33]). Thus, an increase in electron temperature leads to an increase in the instability threshold. For a given pump power, this means a decrease in the threshold density value above which the 100% absorption in the ECR layer becomes possible.

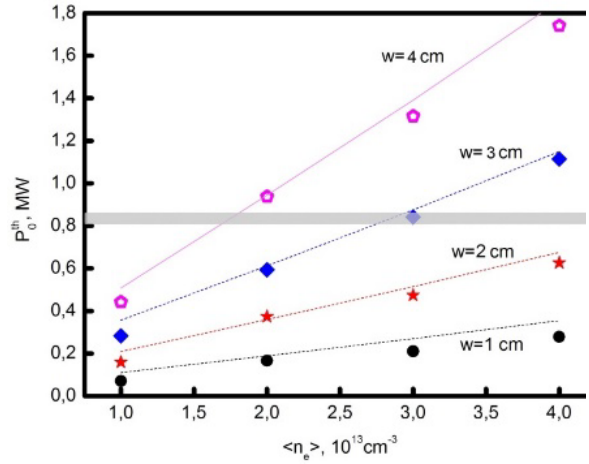

Figure 9. Dependence of the power threshold on the averaged density for different beam widths. The grey line indicates the actual beam power at T-10. For it, the threshold value is $< n_e^{th} > \approx 3 \times 10^{13}$ cm^{-3}.

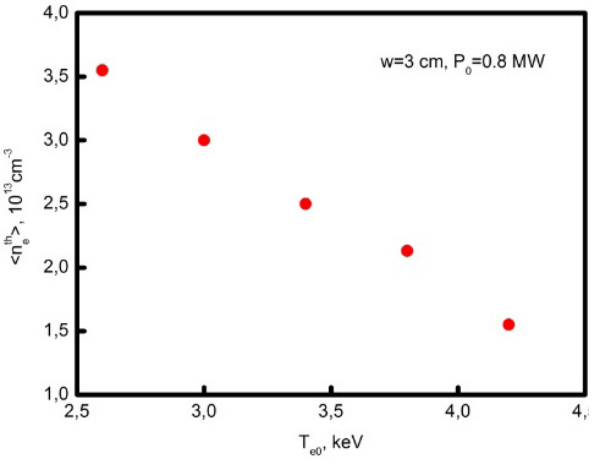

Figure 10. Dependence of the PDI density threshold value on the electron temperature for w = 3 cm and P_0 *= 0.8 MW for the actual T-10 conditions.*

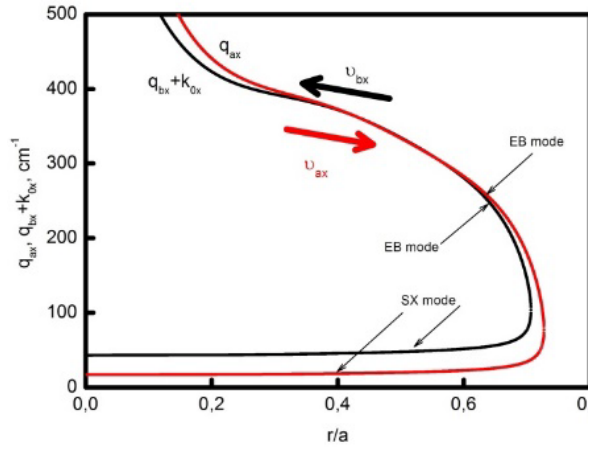

Figure 11. Daughter waves dispersion curves. Arrows correspond to the group velocity sign. Typical TEXTOR conditions.

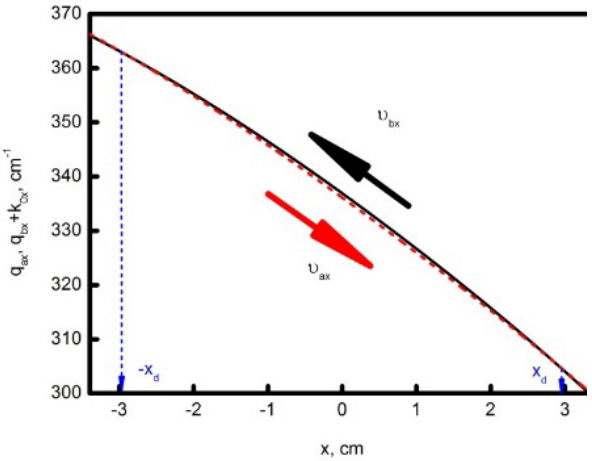

Figure 12. Daughter waves dispersion curves in fine scale. Decay points are $\pm x_d$ *. Typical TEXTOR conditions.*

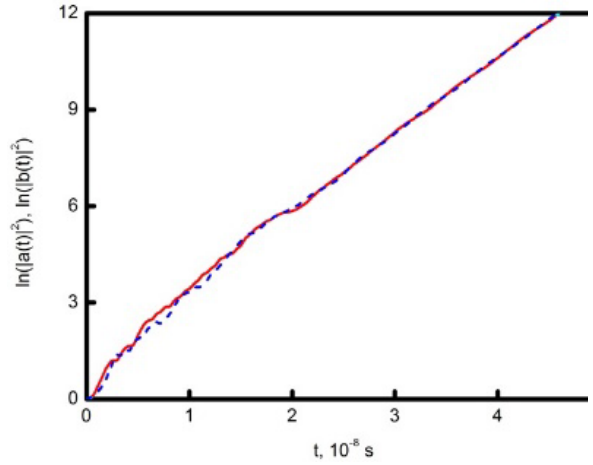

Figure 13. Temporal behavior of the daughter wave amplitudes (see their dispersion curves in fig. 11) shown in semi-exponential scale. Solid red line - $|a(t)|^2$ *, broken blue line -* $|b(t)|^2$ *.*

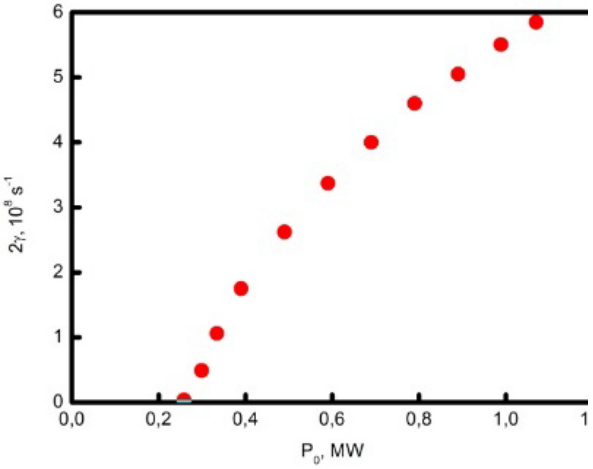

Figure 14. The PDI growth rate versus the pump power for w = 2 cm, 0.245 MW and typical TEXTOR conditions.

3. LOW-THRESHOLD-PARAMETRIC DECAY OF THE PUMP MICROWAVE IN THE TEXTOR TOKAMAK X2-MODE ECRH EXPERIMENTS WITH A MONOTONIC DENSITY PROFILE

The missing power effect in X2-mode on-axis ECRH experiments was also observed at TEXTOR tokamak [18], a medium-sized circular machine with major and minor radii of R = 1.5 m and a = 0.3 m, respectively, and toroidal magnetic field B_T = 2.5 T. A clear heating effect was demonstrated close to the discharge axis where the safety factor was less than one, however the deposited power determined based on the electron temperature and density profiles temporal variation measured by Thomson laser scattering diagnostics appears to be only 200 kW, whereas the launched microwave power was 600 kW [18]. The density profile between the plasma edge and discharge axis was monotonous thus allowing application of the theoretical model developed in this paper to the two-plasmon PDI threshold and growth rate analysis. Dispersion curves of EB daughter waves at frequencies $f_a = 69.79$ GHz and $f_b = 70.21$ GHz are shown in Fig. 11. The latter one is shifted by the wavenumber of the pump at frequency 140 GHz. As it is seen in this figure the decay conditions for three interacting waves are approximately satisfied in a wide plasma region, shown in fine scale in Fig.12. As it is seen in Fig.12, the length of the region between decay points, in which the three-wave interaction takes place is 6 cm. Solution of system (6) shown in Fig.13 for the pump beam width w = 2 cm and power P_0 = 0.4 MW results in exponential growth of the daughter wave amplitudes, indicating the PDI excitation. The PDI growth rate dependence on the pump power is demonstrated in Fig. 14. As it is seen in the figure the PDI takes place at the pump power high than 245 kW. This threshold is substantially lower than the power actually used in the experiment (18). Thus the two-plasmon PDI can be considered as a potential reason of the missing power effect in the TEXTOR X2-mode on-axis ECRH experiment.

4. CONCLUSIONS

In this paper, we have shown that the low-threshold absolute PDI of a pump extraordinary wave can potentially explain the discrepancy between the microwave power launched into the plasma and absorbed in the EC resonance layer, which was found in X2-mode ECRH experiments at the T-10 [19-23] and TEXTOR [18] tokamaks. We have obtained the dependence of the value of the instability threshold on the average density. For density values smaller than the value at which the instability excitation becomes impossible for the given beam power, the instability develops in a suprathreshold regime and can saturate at a high level. The daughter waves leaving the decay layer and gaining a fraction of the pump power experience ECR damping away from the absorption region of the pump wave. As the plasma density increases, the PDI growth rate decreases. Most likely, this results in a decrease in the saturation level of the instability and of the fraction of power gained by the daughter waves. The latter should lead to an increase in the pump power absorbed at the second harmonic of the EC resonance. When the averaged density exceeds a threshold value for the given pump beam power and width, the instability is no longer excited. This allows expecting complete absorption of the pump wave in the second harmonic ECR. The calculated density threshold value appears to be in agreement with the experimentally found threshold of 100% pump power absorption (see figure 12 in [19, 21], figure 4 in [20]). The dependence of the PDI density threshold value $< n_e^{th} >$ on the electron temperature predicted by the theoretical model matches the experimental 100% absorption threshold density dependence on electron temperature shown in figure 3 of [20].
Since the instability threshold for parametric decay of the ordinary pump wave is much higher than the sub-megawatt microwave power used in the O1-mode ECRH experiments at T-10, the pump wave should remain stable. Within the proposed model, this provides an explanation why the heating efficiency in these experiments was in agreement with the theoretical estimate [32].
Altogether, the proposed model provides a qualitative explanation for the discrepancies and dependencies found in ECRH experiments at T-10 [19-23] and TEXTOR.

ACKNOWLEDGEMENTS

The analytical treatment is supported under the RSF 22-12-00010-P grant, the numerical modelling – by the Ioffe Institute contract FFUG -2024-0028 whereas the code for the PDI modeling was developed under the Ioffe Institute contract FFUG -2021-0003. Authors are thankful to Dr. M. Yu. Kantor for providing comments on TEXTOR experimental results.

REFERENCES

[1] ROSENBLUTH, M.N., Phys. Rev. Lett., **29** (1972) 565.
[2] PILIYA, A. D., JETP Letters, **17** (1973) 266.
[3] REIMAN, A., Reviews of Modern Physics, **51** (1979) 311.
[4] COHEN, B. I., COHEN, R. H., NEVINS, W. M., ROGNLIEN, T. D., Reviews of Modern Physics, **63** (1991) 949.
[5] WESTERHOF, E., NIELSEN, S. K., OOSTERBEEK, J. W., SALEWSKI, M., DE BAAR, M. R., BONGERS, W. A., BÜRGER, A., HENNEN, B. A., KORSHOLM, S. B., LEIPOLD, F., MOSEEV, D., STEJNER, M., THOEN, D.J., Phys. Rev. Lett., **103** (2009) 125001.
[6] NIELSEN, S. K., SALEWSKI, M., WESTERHOF, E., BONGERS, W., KORSHOLM, S. B., LEIPOLD, F., OOSTERBEEK, J. W., MOSEEV, D., STEJNER, M., Plasma Phys. Control. Fusion, **55** (2013)115003.
[7] HANSEN, S. K., NIELSEN, S. K., STOBER, J., RASMUSSEN, J., STEJNER, M., HOELZL, M., JENSEN, T., Nucl. Fusion, **60** (2020) 106008.
[8] HANSEN, S. K., JACOBSEN, A. S., WILLENSDORFER, M., NIELSEN, S. K., STOBER, J., HÖFLER, K., MARASCHEK, M., FISCHER, R., DUNNE, M., THE EURO FUSION MST TEAM AND THE ASDEX UPGRADE TEAM, Plasma Phys. Control. Fusion, **63** (2021) 095002.
[9] TANCETTI, A., NIELSEN, S. K., RASMUSSEN, J., GUSAKOV, E. Z., POPOV, A. Y., MOSEEV, D., STANGE, T., SENSTIUS, M. G., KILLER, C., VECSEI, M., JENSEN, T., ZANINI, M., ABRAMOVIC, I., STEJNER, M., ANDA, G., DUNAI, D., ZOLETNIK , S., LAQUA, H., Nuclear Fusion, **62** (2022) 074003.
[10] TANCETTI, A., NIELSEN, S. K., RASMUSSEN, J., MOSEEV, D., STANGE, T., THE W7-X TEAM, Plasma Phys. Control. Fusion, **65** (2023) 015001.
[11] CLOD, A., SENSTIUS, M. G., NIELSEN, A. H., RAGONA, R., THRYSØE, A. S., KUMAR, U., CODA, S., NIELSEN, S. K., Physical Review Letters, **132** (2024) 135101.
[12] CODA, S., Nuclear Fusion, **55** (2015) 104004.
[13] ZURRO, B., BACIERO, A., TRIBALDOS, V., LINIERS, M., CAPPA, A., LOPEZ-FRAGUAS, A., JIMENEZ-REY, D., FONTDECABA, J. M., NEKHAIEVA, O., THE TJ-II TEAM, Nucl. Fusion, **53** (2013) 083017.
[14] MARTÍNEZ, M., ZURRO, B., BACIERO, A., JIMÉNEZ-REY, D., TRIBALDOS, V., Plasma Phys. Control. Fusion, **60** (2018) 025024.
[15] ANDREEV, V. F., DNESTROVSKIJ, YU. N., OSSIPENKO, M. V., RAZUMOVA, K. A., SUSHKOV, A. V., Plasma Phys. Control. Fusion, **46** (2004) 319.
[16] SLIEF, J. H., VAN KAMPEN, R. J. R., BROOKMAN, M. W., VAN DIJK, J., WESTERHOF, E., VAN BERKEL, M., Nucl. Fusion **63**, (2023) 026029.
[17] GUSAKOV, E. Z., POPOV, A. Y., MESHCHERYAKOV, A. I., GRISHINA, I. A., TERESHCHENKO, M. A., Phys. Plasmas, **30** (2023) 122112.
[18] KANTOR, M. YU., BERTSCHINGER, G., BOHM, P., BUERGER, A., DONNÉ, A.J.H., JASPERS, R., KRÄMER-FLECKEN, A., MANN, S., SOLDATOV, S., ZANG QING AND THE TEXTOR TEAM, Proc. of 36th EPS Conference on Plasma Phys., Sofia, June 29 - July 3, 2009 ECA Vol.**33E**, P-1.184 (2009).
[19] DNESTROVSKIJ, YU. N., DANILOV, A. V., DNESTROVSKIJ, A. YU., KLYUCHNIKOV, L. A., LYSENKO, S. E., MELNIKOV, A. V., NEMETS, A. R.**,** NURGALIEV, M. R., SUBBOTIN, G. F., SOLOVEV, N. A., SUSHKOV, A. V., SYCHUGOV, D.YU., CHERKASOV, S. V., Plasma Physics Reports, **46** (2020) 477.
[20] DNESTROVSKIJ, Y. N., DANILOV, A. V., DNESTROVSKIJ, A. YU., LYSENKO, S. E., MELNIKOV, A. V., NEMETS, A. R., NURGALIEV, M. R., SUBBOTIN, G. F., SOLOVEV, N. A., SYCHUGOV, D. YU., CHERKASOV, S. V., Plasma Phys. Control. Fusion, **63** (2021) 055012.
[21] DNESTROVSKIJ, Y. N., MELNIKOV, A. V., LOPEZ-BRUNA, D., DNESTROVSKIJ, A. Y., CHERKASOV, S. V., DANILOV, A. V., ELISEEV, L. G., KHABANOV, F. O., LYSENKO, S. E., SYCHUGOV, D. Y., Plasma Phys. Control. Fusion, **65** (2023) 015011.
[22] DNESTROVSKIJ, Y. N., MELNIKOV, A. V., ANDREEV, V. F., LYSENKO, S. E., NURGALIEV, M. R., SHALASHOV, A. G., JETP Letters, **118** (2023) 255.
[23] DNESTROVSKIJ, Y. N., MELNIKOV, A. V., ANDREEV, V. F., LYSENKO, S. E., NURGALIEV, M. R., SHALASHOV, A. G., Proc. of 51th International Conference on Plasma Physics and CF, March 18 – 22, 2024, Zvenigorod (DOI: 10.34854/ICPAF.51.2024.1.1.032).
[24] GUSAKOV, E. Z., POPOV, A. Y., Phys. Usp., **63** (2020) 365.
[25] GUSAKOV, E. Z., POPOV, A. Y., Physics of Plasmas, **23** (2016) 082503.
[26] GUSAKOV, E. Z., POPOV, A. Y., TRETINNIKOV, P. V., Nucl. Fusion, **59** (2019) 106040.
[27] GUSAKOV, E. Z., POPOV, A. Y., Plasma Physics Reports, **49** (2023) 949.
[28] GUSAKOV, E. Z., POPOV, A. Y., Plasma Physics Reports, **49** (2023) 194.
[29] POPOV, A. Y., GUSAKOV, E. Z., Phys. Plasmas, **31** (2024) 072104.
[30] POPOV, A. Y., GUSAKOV, E. Z., Plasma Physics Reports, **51** (2025) 118.
[31] POPOV, A. Y., NAGOVITSYN, A. A., GUSAKOV, E. Z., Phys. Plasmas, **31** (2024) 120701.
[32] PILIYA, A. D., FEDOROV, V. I., Reviews of Plasma Physics, **13** (1987) 335.
[33] GUSAKOV, E. Z., POPOV, A. Y., TRETINNIKOV, P. V., Plasma Phys. Control. Fusion, **61** (2019) 085008.
[34] ANDREEV, V. F., BORSCHEGOVSKIJ, A. A., CHISTYAKOV, V. V., DNESTROVSKIJ, Y. N., GORBUNOV, E. P., KASYANOVA, N. V., LYSENKO, S. E., MELNIKOV, A. V., MYALTON, T. B., ROY, I. N., SERGEEV, D. S., ZENIN, V. N., Plasma Phys. Control. Fusion, **58** (2016) 055008.